Combination of PAT and mechanistic modeling tools in a fully continuous powder to granule line: Rapid and deep process understanding

András Domokos [a], Éva Pusztai [b], Lajos Madarász [a], Brigitta Nagy [a], Martin Gyürkés [a], Attila Farkas [a], Gergő Fülöp [a], Tibor Casian [c], Botond Szilágyi [d,*,1,2], Zsombor Kristóf Nagy [a,*,1,2]

[a] Budapest University of Technology and Economics, Organic Chemistry and Technology Department, H-1111 Budapest, Hungary
[b] Budapest University of Technology and Economics, Department of Chemical and Environmental Process Engineering, H-1111 Budapest, Hungary
[c] Department of Pharmaceutical Technology and Biopharmacy, "Iuliu Hatieganu" University of Medicine and Pharmacy, 400012 Cluj-Napoca, Romania
[d] Budapest University of Technology and Economics, Faculty of Chemical Technology and Biotechnology, H-1111 Budapest, Hungary

ARTICLE INFO

ABSTRACT

Comprehensive understanding of an integrated continuous pharmaceutical technology was achieved in this study by a combining design of experiments and mechanistic modeling-based simulations. The powder to granule line consisted of twin-screw wet granulation, vibrational fluid-bed drying and milling. A Partial Least Squares (PLS) regression model was built using Near-infrared (NIR) spectroscopy for the real-time monitoring of the product moisture content after the milling step. A split-plot full factorial experimental design was set up and executed to help the understanding of the relationships between the moisture content and process parameters. Furthermore, a mechanistic model was built, involving heat transfer between the drying air and the solid material. The unknown kinetic model parameters were estimated using the results of the experimental study resulting in good calibration and validation performance. The simulations not only reinforced the experimental observations but also paves the way for model-based process monitoring and optimal control.

© 2021 The Author(s). Published by Elsevier B.V. This is an open access article under the CC BY license (http://creativecommons.org/licenses/by/4.0/).

1. Introduction

Continuous manufacturing (CM) has gained significant attention in the pharmaceutical industry in the recent years [1–3]. Technology transfer from batch to continuous faces dosage (*e.g.* tablets, injectables, *etc.*) and unit-operation specific challenges as well. Regarding the product form, approximately 80% of the pharmaceuticals are solid dosage formulations, the majority of them being tablets [4]. Within the solid form production, granulation is critical for the improvement of powder properties *e.g.* flowability required for the tableting process operation [5,6]. Several process variant is known in the literature [7], among which wet granulation (when a liquid is applied to help stick the small particles of the starting powder blend together) has become the most common approach due to the very good controllability and reproducibility [8]. Thus, implementing wet granulation in a continuous manner recently gained significant attention [9]. Numerous papers investigate continuous twin-screw wet granulation (TSWG) and the effect of process parameters on product quality [10–22].

Wet granulation is inherently followed by drying to eliminate the residual granulating liquid from the granule product [23]. The challenge of drying is that high operating temperatures might result in thermal decomposition of the API, conversely, low-temperature drying might fail to meet the established limit with reasonable drying time. Various dryer constructions are available to overcome these issues. Fluidized bed drying (FBD) is a frequently applied technology, which applies heated air flowing through the wet granules [24]. The continuous implementation of FBD is represented in the literature mainly by segmented, semi-continuous FBDs developed by GEA [25–27], Glatt [24,28,29], or Bohle [30]. In these systems, the wet granules are collected and dried in separated compartments in small batches, and the residence time and batch size are defined by the rotation frequency of the compartments. Truly continuous horizontal bed dryers have long been known in the food industry [31,32]. In these systems, the vibration of the perforated bed triggers forward particle movement, meanwhile the drying air flows through the mesh enabling significantly more control over the process, translating to reduced quality variability. Bohle presented such a continuous dryer for pharmaceutical materials, which was integrated with continuous TSWG as well [33].

Continuous manufacturing is a promising alternative for the pharmaceutical industry and offer great overall benefits. However, in order to identify and remove the off-spec products effectively

* Corresponding authors.
E-mail addresses: szilagyi.botond@vbk.bme.hu (B. Szilágyi), zsknagy@oct.bme.hu (Z.K. Nagy).
[1] Joint last co-authorship.
[2] Postal address: 3 Műegyetem rkp., H-1111 Budapest, Hungary.

from the stream and to improve the safety and quality tight, real-time monitoring is required by Process Analytical Technologies (PATs) [34–36]. Various PAT tools can be applied to monitor the critical quality attributes (CQA) of the TSWG and FBD products, such as particle size and shape [37], blend uniformity [38,39], polymorphism [40], or the moisture content of the granules [4,30,41–44]. The importance of a comprehensive PAT network is even higher in integrated systems, where the disturbances can propagate through the production line, sometimes generating complex and delayed effects [45] Only a handful of examples can be found in the literature for integrated TSWG-FBD systems with incorporated PAT tools for real-time CQA monitoring. NIR spectroscopy was utilized for real-time moisture content measurement in the Consigma™ system by Chablani et al. [42] and by Fonteyne et al. [4,41,43], in the Glatt GPCG2 CM system by Pauli et al. [24] and in the Bohle BCD 25 system by Peters et al. [30]. The first fully continuous powder-to-granule line was published recently by the authors for the production of ultra-low dose granules, in which however no PAT tools were incorporated for real-time monitoring yet [46].

Besides PAT-based monitoring, another tool for getting new traction in the process design, operation and analysis is mathematical modeling and numerical simulations [44,47]. Traditionally, the models were used for numerical experimentation, model-based analysis, design and predictive control or execution of *in-silico* Design of Experiment (DoE) studies, resulting in cost and considerable material savings [48]. With the quick spread of PAT tools combined with the ongoing cross-industry digitalization efforts, novel applications for the simulations were also found, such as the digital twins [49], when the simulation utilizes real-time process data. Digital twins can be used for on-line fault diagnosis or as soft-sensor granting access to a high amount of real-time process- and product-related information. Model calibration and validation with quantified parametric uncertainty are critical to ensure reliable predictions in those applications [50]. Several pharmaceutical drying processes were modeled successfully, *e.g.* the Consigma™ line [51] or the continuous vibrated FBD of Bohle [50].

As it was presented, deep process understanding of integrated continuous technologies is possible through the implementation of PAT tools and model-based digital twins. However, no example was found for such a process design in the case of fully continuous TSWG-FBD lines. Hence, in this work our aim was to extend the investigations of the system presented in [46], aiming for a detailed, systematic and comprehensive modeling-experimental analysis of product moisture content. To achieve this, firstly, a PLS-based NIR technique was developed for real-time moisture content monitoring. Then, the effects of process parameters on the product moisture content were systematically analyzed by a full factorial split-plot experimental design. Furthermore, a mechanistic drying model was developed, which was able to predict the moisture content generally within the measurement uncertainty and enabled to carry out simulation studies. Since very few examples can be found in the literature about truly continuous TSWG-FBD-milling lines, the presented PAT- and model-based approach of system performance evaluation can be very useful for the deeper understanding of these processes.

2. Materials and methods

2.1. Materials

For the granulation experiments, α-lactose monohydrate (Granu-Lac® 70) and corn starch were applied in the starting powder blend. The α-lactose was supplied by Meggle Pharma (Wasserburg, Germany) and corn starch was provided by Roquette Pharma (Lestrem, France). Purified water was used as granulating liquid with Kollidon® 30 (Povidone, PVPK30) as a binder, shipped by BASF (Ludwigshafen, Germany).

2.2. Granulation experiments

The continuous production of granules was carried out in an integrated TSWG-FBD-milling manufacturing line. A continuous twin-screw multipurpose equipment, TS16 QuickExtruder® (Quick 2000 Ltd., Hungary) was applied for wet granulation. A screw with 16 mm diameter (25 L/D ratio) was used with a set screw configuration consisting of conveying and two kneading zones (Fig. S 1). The kneading zones comprised individual elements set up at a 45° angle with a forward configuration (first zone: 5 elements; second zone: 5 elements).

A pre-blend of α-lactose and corn starch was applied as a starting powder. Pre-blending was carried out *via* manual mixing in plastic bags for 5 min. The pre-blend was fed into the system by a gravimetric feeder (Brabender Technologie, Duisburg, Germany) at the first zone of the granulator. The granulating liquid was prepared by dissolving PVPK30 in purified water (ratio: 75 g in 200 mL) and was dosed into the second zone (upstream of the first kneading zone) using a peristaltic pump (Watson-Marlow 120 U, Wilmington, MA, US) with silicone tubing (inner diameter: 3.1 mm). The mass flow rate of the pre-blend was varied between 1 and 3 kg/h, while the liquid dosing was set in a range of 1.33–4.67 g/min, according to the liquid to solid ration (L/S) setting of the actual experiment (0.08–0.14). The peristaltic pump was calibrated with the granulation liquid prior to the experiments. The screw speed was set according to the mass flow of the pre-blend: 200 rpm for 1 kg/h, 300 rpm for 1.5 kg/h and 400 rpm for 2 kg/h. The setup of TSWG is shown in Fig. S 2 with the pre-blend and granulation liquid feeders, the twin-screw device and the inlet of the continuous dryer right under the screw tips.

2.3. Continuous drying

The continuous drying of the wet granules was carried out in a horizontal FBD (Quick 2000 Ltd., Hungary) (Fig. 1). The main element of the device was a perforated metal mesh, which was vibrated by vibromotors with a constant frequency of 50 Hz. The wet granules fell from the screw tips directly onto this bed and started moving towards the other end of the apparatus as a result of the vibration. Drying took place during this movement, as heated air was flowing upwards from the metal mesh and through the granules. The vibrating bed was divided into 4 drying zones, each with its corresponding filter bag above the granules. Heating could be applied on the inlet air in the first 3 zones individually, while the last, 4th zone was only for conditioning with room temperature air flow. The air flow rate could be set independently for all of the 4 zones. It is important to note that real fluidization did not take place in the applied air flow range of the device. Automatic filter bag dedusting happened once in a minute. The temperature of the drying air was varied between 30 and 90 °C, while the applied range of the flow rate was 60–120 L/min per zones. The schematic drawing of the continuous dryer is presented in Fig. 1.

2.4. Milling

A continuous mill (Quick 2000 Ltd., Hungary) was placed under the outlet of the continuous dryer, which could be operated either with a co-mill or an oscillatory mill tool (Fig. S 3). The dried granules fell directly into the mill. Oscillatory milling with 1 mm sieve size was applied in all experiments. Milling intensity was set to 200 oscillations/min in all cases.

2.5. Granule characterization – residual moisture content

The amount of remaining water in the dried and milled product was determined by loss on drying (LOD, % w/w) measurements. Samples were taken from the material exiting the continuous mill, and were put in an oven for 60 min at 105 °C. The sample mass was measured
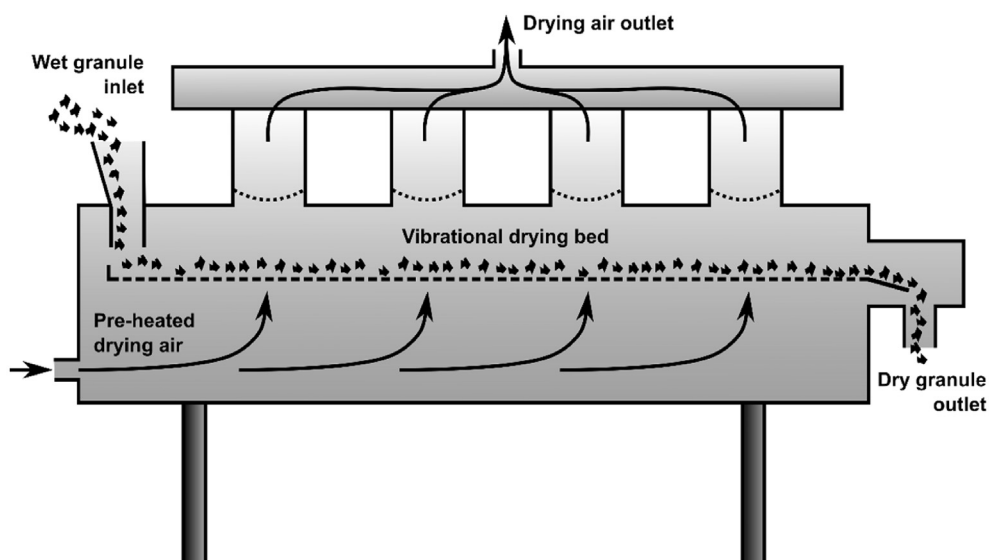
Fig. 1. The schematic drawing of the continuous vibrational fluidized-bed dryer used during the experiments.

using an analytical scale before and right after the 60 min of drying, and the LOD was calculated from the difference.

2.6. NIR spectroscopy and spectral evaluation

A Bruker MPA FT-NIR (Bruker Optik GmbH, Ettlingen, Germany) spectrometer, equipped with a Solvias fiberoptic probe was used for real-time moisture content measurement of the dried and milled material. A vibratory conveying feeder (Fritsch Laborette 24, Idar-Oberstein, Germany) with a U-shaped channel was positioned under the outlet of the milling device, and the NIR probe was fixed above the channel of the vibratory feeder (Fig. 2). Thus, the NIR spectra was collected from the continuously moving material. Spectra collection was carried out in reflection mode, and each NIR spectrum was collected by accumulating 8 scans with 8 cm^{-1} resolution in the range of 4000–12,500 cm^{-1}. Spectrum accumulation was completed using OPUS® 7.5 software (Bruker), while the real-time evaluation of the spectra was carried out using MATLAB 9.7. (MathWorks, USA) and PLS Toolbox 8.7.1.
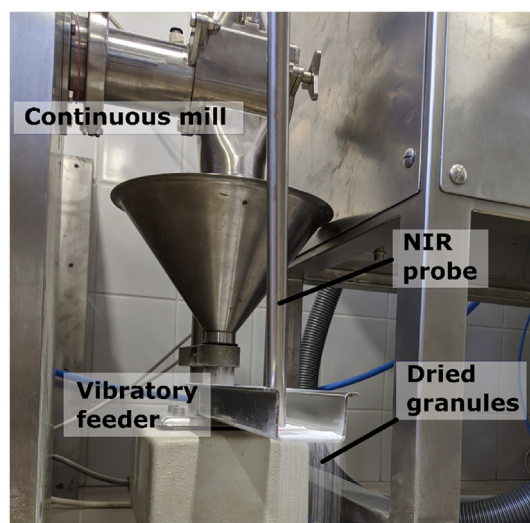

Fig. 2. Experimental setup for in-line moisture content measurement using NIR spectroscopy.

(Eigenvector Research, USA). A Matlab script and an interface have been developed to import the spectra to Matlab in real-time. After that, another script was used for the chemometric moisture content determination using a Partial Least Squares (PLS) model developed in PLS Toolbox (also in real-time). During building of the PLS model, the preprocessing of the spectra consisted of Savitzky-Golay smoothing (2nd order polynomial, 15-point window), Standard Normal Variation (SNV) correction and mean centering. Venetian blinds cross-validation method was applied with 10 data splits and 1 left-out sample per blind.

2.7. Design of experiments with the integrated continuous system

The previously described three stages of the continuous system were operated in an integrated fashion: the wet granules produced during TSWG fell directly into the continuous FBD, and the continuous mill was connected to the outlet of the drier as well. Then, the dried and milled material was conveyed with a vibratory feeder, and by fixing the NIR probe above the channel of the feeder in-line spectra were collected for real-time moisture content analysis.

A Split-Plot DoE study was created for the systematical evaluation of the effect of different process parameters on the moisture content of the produced granules. The examined parameters were the mass flow rate of the pre-blend, the liquid to solid ratio (L/S), and the temperature and flow rate of the drying air. Each factor was varied on two levels, and with multiple repeats at the central point. The temperature of the drier was a so-called "hard-to-change factor" since quite a long time was required for a new setting to stabilize. Thus, executing the experiments with the temperature settings in randomized order would have resulted in a drastically elongated measurement time. Instead, the DoE was split up into blocks according to the temperature levels (split-plot design). Each block was repeated twice to separate the variability of the change of temperature from the variability originating from the restricted randomization. Central point experiments were conducted between the blocks, resulting in a total of 4 central point repeats. The set levels of the process parameters are listed in Table 1, while the order of the experiments executed in the final DoE is presented in Appendix 1 in Table S1.

The temperature of the granulator was kept constant at 25 °C in all cases. The temperature and the flow rate of the drying air in the continuous dryer could be set for each of the 4 zones individually (except for the temperature of the 4th zone as detailed in Section 2.3), which would have increased the number of parameters significantly. Thus, in

Table 1
The set levels of process parameters in the DoE study for the evaluation of the effect of process parameters on the moisture content of the product.

Level of process parameter	Drying temperature (°C)	Drying air flow rate/zone (L/min)	Mass flow rate (kg/h)	L/S (−)
Lower	30	60	1.0	0.08
Higher	50	120	2.0	0.14
Central point	40	90	1.5	0.11

this study, the first 3 drying zones were handled together by setting the air temperature and flow rate to the same level between 30 and 50 °C and 60 and 120 L/min. In the case of the 4th zone, the air flow rate was set to 60 L/min in each experiment. The results were evaluated with analysis of variance (ANOVA) using the TIBCO Statistica (Version 13.5) software.

The experimental design was carried out in one long operational run. The system was initiated with the central point settings (1.5 kg/h, 0.11 L/S, 40 °C, 90 L/min), and the in-line NIR measurement was started simultaneously. The recorded spectra were analyzed in real-time, thus the moisture content trend could be followed accurately. At the beginning of the experiment, the system was operated for *ca.* 20 min to reach steady the state in all units (the stabilization of the drying temperature took most of this time, a few minutes was enough for the other units and parameters). When the in-line signal stabilized, the actual moisture content was noted, and we moved on to the next setting within the first temperature block. The system was operated at each setting for approximately 5–10 min to reach the steady state, which was determined based on visual observation and the in-line NIR measurement. In each setting, 5 spectra were marked to determine the actual residual solvent content level. After finishing a temperature block, a slightly longer settling time was required to reach the steady temperature of the next block (20–30 min). An overall operating time of *ca.* 5 h was required to execute the experimental design, which was quite impressive taking into account the number of settings [36].

After evaluating the results of the presented experimental design, the temperature factor was found to be statistically not significant (see later in Section 3.2). As temperature has an important role in drying mechanism [48], the experimental plan presented in Table 1 was supplemented with subsequent levels for drying temperature at 70 and 90 °C as new blocks in order to gain more insight into the effect of this parameter. The investigated range of the rest of parameters was identical to the previously presented DoE setup. The exact settings are listed in Appendix 1 in Table S 2.

2.8. Modeling of the continuous drying process

The drying models can be divided into two major categories: the equilibrium and the Arrhenius concepts [52]. The former assumes heat transfer limitation between the drying air and the particles [53], whereas the latter considers that the drying process is governed by the evaporation rate. In this work, the Arrhenius approach is employed. The developed model distinguishes a gas and a solid phase. Although there is also liquid in the system in the form of moisture, this is handled as an intrinsic property of the pseudo-solid phase. The sub-processes considered in the drying model are illustrated in Fig. 3, where it seems that the particles are not separated from each other. Instead, there are channels in the air flow, reducing the overall solid surface area and making the liquid diffusion from the pores to the surface a macroscopically significant step.

Under such conditions, two drying regimes exist: above a critical moisture content (X_C) the drying rate (R_V) is independent of the actual moisture (X). Below X_C, the liquid is transferred to the surface of the particles from the inner pores first and then is evaporated, which translates to a moisture content-dependent drying rate. These are described with the semi-empirical Eq. [54]:

$$R_v = \begin{cases} k(1-H_r), \text{if } X > X_c \\ k(1-H_r)\dfrac{X}{X_c}, \text{if } X < X_c \end{cases} \tag{1}$$
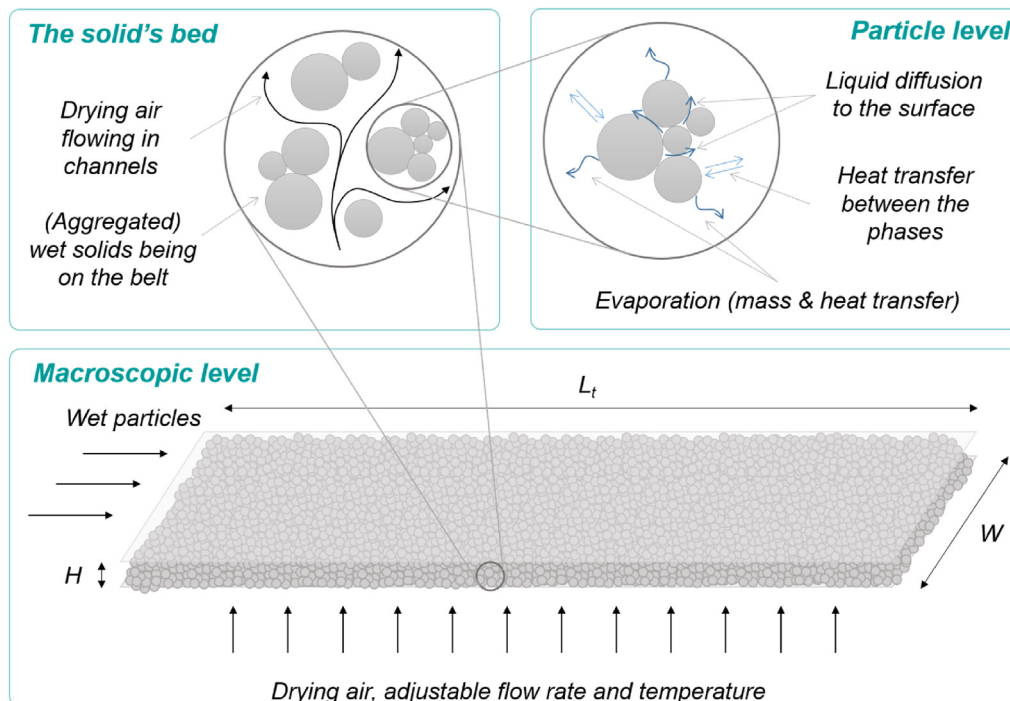

Fig. 3. The main effects considered in the drying model in macroscopic scale and the level of particles.
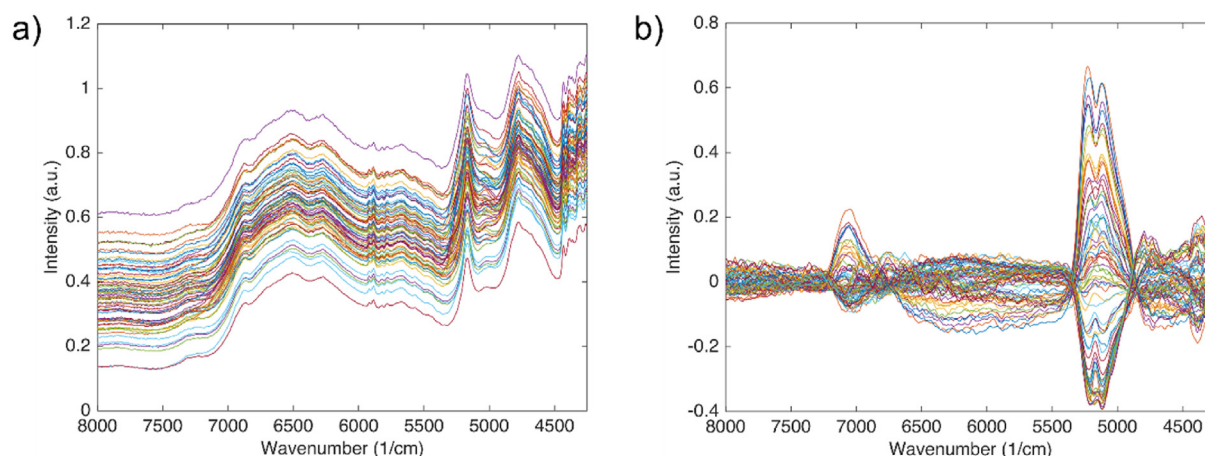
Fig. 4. In-line collected NIR spectra of granules with different moisture content before (a) and after (b) preprocessing.

k is the temperature-dependent rate constant ($T_{K,s}$: solid temperature in Kelvin), expressed as:

$$k = k_0 \exp\left(-\frac{E_A}{RT_{K,s}}\right) \qquad (2)$$

In Eq. (1) H_r denotes the relative humidity, accounting that the drying rate is negatively proportional to the relative humidity. H_r is expressed as the ratio of actual partial pressure (P_A) and saturation pressure at the given temperature (P_A^*):

$$H_r = \frac{P_A}{P_A^*} \qquad (3)$$

The evaporation is accompanied by the release of evaporation heat, resulting in the decrease of solid temperature (T_s) as well as the increase of the relative humidity of the air. The solid-gas heat transfer compensates evaporation heat, described as a function of temperatures, heat transfer coefficient (U) and apparent heat transfer area (A):

$$Q = UA(T_s - T_a) \qquad (4)$$

where T_a is the air temperature in the bed.

The developed process model assumes that the gas phase is well-mixed, and the heat of evaporation is completely absorbed by the solids. Then, a differential equation system with four states, namely the air temperature (T_a), partial pressure of water (P_A), the solid temperature (T_s) and moisture content (X), is derived, which is described in detail in Appendix 2. The numerical solution of the model-equations was performed in MATLAB R2019a using an explicit Runge-Kutta method by calling the *ode23* function.

The heat transfer coefficient (U), activation energy (E_A) and evaporation rate constant (k) are unknowns for this system, hence, has to be determined based on the experimental data. The parameter identification is carried out by optimization, with the decision variable vector of $\boldsymbol{\theta} = (U, E_A, k)$ as:

$$\min_{\boldsymbol{\theta}} \varphi(\boldsymbol{\theta}) \qquad (5)$$

where φ denotes the objective function, depending on the experimentally measured (X_e) and simulated (X_s) steady state moisture contents of the product of the N calibration experiments.

$$\varphi(\boldsymbol{\theta}) = \frac{1}{N} \sum_{i=1}^{N} \left[(X_{s,i} - X_{e,i})^2 \right] \qquad (6)$$

90% of the experiments were randomly selected for model calibration, the remaining 10% was used for validation. 10% of experiments

translated to 3 validation experiments, which is in the commonly used range of pharmaceutical model validations [55–57]. Maximizing the number of calibration experiments is known to contribute to the mitigation of parameter uncertainties and inter-correlations.The optimization was solved using the covariance matrix adaptation-evolution strategy (CMA-ES) global optimization algorithm [58], and the statistics (parameter covariance matrix and the 95% confidence intervals) were calculated by executing a nonlinear regression using the *lsqnonlin* function, started from the point returned by the global optimization. The confidence intervals were calculated by *nlparci* function, using the decision variable vector, vector of residuals and the Jacobian matrix returned by the *lsqnonlin*. To quantify the effects of uncertainties, firstly, 2000 random kinetic parameter combinations were generated by Monte-Carlo sampling from the uncertainty space. Then, the process was simulated using these random parameters, which not only allows the calculation of the mean and the standard deviation (SD) of the simulated outputs but also permits the construction of a full probability distribution [59].

3. Results and discussion

3.1. Development of PLS model for in-line moisture content measurement by NIR

An NIR probe was positioned above the channel of the vibratory feeder, which conveyed the dried and milled material produced in the integrated continuous system. Spectra were collected continuously every 8 s from the moving material, and by taking samples for off-line LOD measurements, the relationship between the spectra and the moisture content of the product could be determined. The spectra taken during the sampling were marked to be used for calibration. The calibration was carried out by varying the L/S ratio (0.07–0.16) and the drying air flow rate (45 L/min-140 L/min) to cover a wide range of moisture content for calibration. The mass feeding rate was set to 1 kg/h, the temperature to 25 °C (no heating was applied). This way, a residual solvent content range of approximately from 0.5% to 7% could be covered. The spectra of the completely dry material were also obtained from samples just taken out of the drying oven, which were used as 0% calibration samples.

After preliminary studies of the optimal spectral range and preprocessing methods, the spectral range of 8000–4250 cm^{-1} was selected for calibration. The raw and pre-processed spectra are shown in Fig. 4a and b. As it can be seen, the spectral regions of 5300–4900 cm^{-1} and 7200–6700 cm^{-1} contained the majority of information about the amount of residual granulating liquid in the product, which was in good agreement with the main NIR absorption regions of water [60].
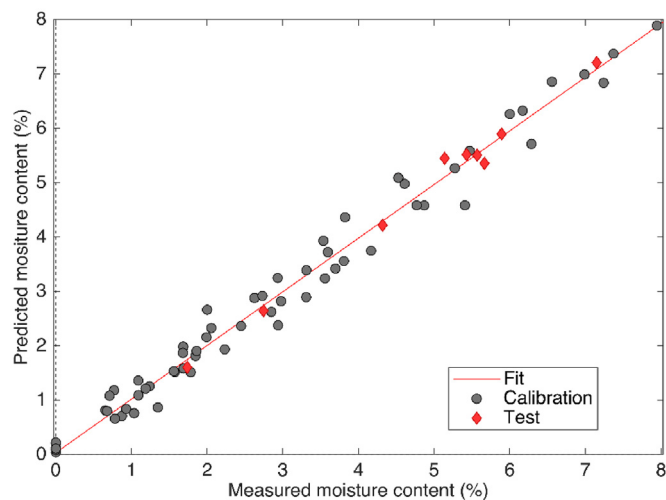
Fig. 5. PLS calibration built for the in-line measurement of granule moisture content. Calibration samples are marked with grey, while validation samples are marked with red color ($R^2_{prediction}$ = 0.99089). (For interpretation of the references to color in this figure legend, the reader is referred to the web version of this article.)

Fig. 6. Continuous experiment: performance of the in-line NIR measurement. The numbers correspond to the settings detailed in Table 2.

Table 2
Parameter settings of the continuous experiment in Fig. 6.

Setting	Drying temperature (°C)	Mass flow rate (kg/h)	Drying air flow rate (L/min)	L/S (−)
1.	40	1.5	90	0.11
2.	40	2	120	0.08
3.	40	2	60	0.12
4.	40	1	120	0.09
5.	40	1	60	0.10
6.	40	1.5	90	0.11

A PLS model was built using the preprocessed NIR spectra and the reference off-line LOD measurements. Altogether 70 spectra were included in the final model, and 4 latent variables were applied, which explained 98.39% of the variation. An experiment was executed independently from the calibration to generate data for validation, from which 9 samples were used (Fig. 5). With these settings, the error of calibration (RMSEC) and cross-validation (RMSECV) were 0.278 and 0.334, respectively. The error of prediction in the validation experiment was RMSEP = 0.168, which showed the robustness of the model and the applicability for in-line monitoring of the continuous process.

In order to test the developed in-line measurement tool, experiments were carried out using the continuous system with the incorporated NIR probe. The process parameters were changed within the range of the calibration and the product moisture content was monitored in real-time. The parameter settings of the experiment are shown in Table 2, and the moisture content results with the corresponding settings are shown in Fig. 6.

It was found that the start-up period was approximately 10 min, followed by the steady state, where a low fluctuation of the moisture content was observed. At 20 min the malfunction of the gravimetric feeder (used for the pre-blend feeding) caused a disturbance, but the signal stabilized quickly after the restart of the device. The parameter settings were changed shortly after reaching the steady state again (at 34 min in Fig. 6). The system response was found to be sharp, and the signal stabilized quickly. Then, the remaining settings detailed in Table 2 were tested in the system having *ca.* 20 min at each setup. Another accidental stoppage of the gravimetric feeder could be detected in the moisture content signal (at ~70 min), followed by rapid re-stabilization.
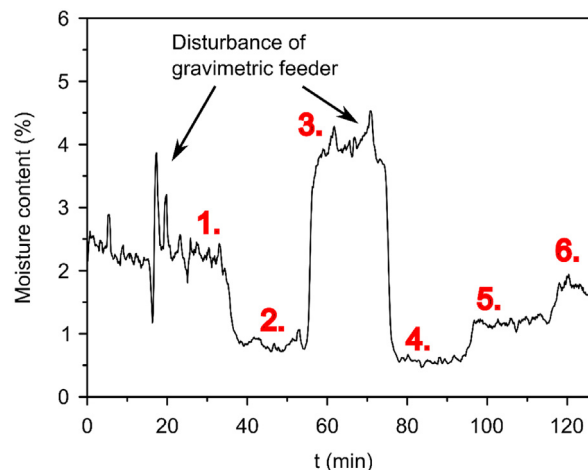
Based on the result of the experiments, the developed in-line NIR method was suitable for real-time system monitoring by detecting the varying moisture content associated with the changes of the operating parameters, and even minor fluctuations could be detected. Thus, the in-line method was suitable to be applied as measurement tool during the execution of the split-plot experimental design.

3.2. Evaluation of the system performance by DoE

The split-plot experimental design detailed in Table 1 (Section 2.7) was used to assess the effect of the mass flow rate of the pre-blend, the L/S, and the temperature and the flow rate of drying air on the moisture content of the granules. The results are shown in a variability plot in Fig. 7.

In Fig. 7 a small triangle marks an individual setting, the corresponding parameter levels can be found beneath the figure (the data are not arranged according to the execution order of the experiments, which is shown in Table S 1). As it can be seen, each setting was repeated twice, whereas four central point repeats were conducted. The repeatability of the experiments was found to be good according to these central point measurements, carried out at the beginning of the operation and between the temperature blocks (visible on the first column of Fig. 7). Based on the visual evaluation, the L/S ratio has the greatest influence on the moisture content, which results are shown within the yellow, dash-dotted rectangles. Substantial differences can be observed in the measured moisture content between the lower (1.42%) and higher (3.09%) L/S levels. Moreover, in a few cases, the results of the two repeats were not as close as at the central point, which was observed mainly at the higher L/S level (0.14). This phenomenon can be explained by the disturbances in the feeding flow rate of the pre-blend due to the inaccuracies of the gravimetric feeder. At this high level of moisture content, a small variation in the pre-blend mass flow could have resulted in hardly processable over-wetted particles, which showed different drying behavior.

The mass flow rate and the drying air flow rate were also found to be important. The effect of these variables is shown within the green (dotted line) and red (dashed line) rectangles in Fig. 7, respectively. The lower level of mass flow rate and the higher level of drying air flow rate resulted in notably dryer material. In Fig. 7, the blue (solid line) rectangles include the repeats on the two temperature levels. The results obtained at the higher and lower levels of this factor did not differ as much as in the case of the other three factors. The residual solvent content was reduced below 1% even with 30 °C (1 kg/h, 0.08 L/S, 120
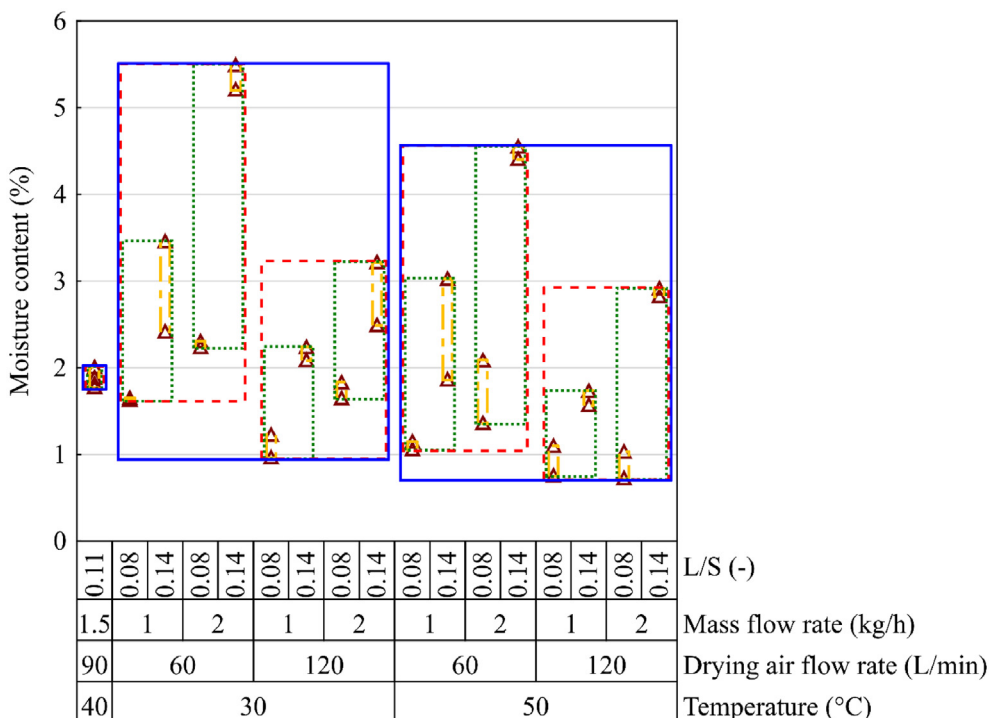
Fig. 7. Variability plot presenting the results of the split-plot experimental design. Each setting is marked with a triangle, and the colored rectangles represent the higher and lower levels of the examined parameters (L/S: yellow rectangle with dash-dotted line; mass flow rate: green rectangle, dotted line; drying air flow rate: red rectangle, dashed line; temperature: blue rectangle, solid line). (For interpretation of the references to color in this figure legend, the reader is referred to the web version of this article.)

L/min), but 50 °C could not decrease moisture content below 4% with 2 kg/h, 0.14 L/S and 60 L/min.

The statistical analysis of the results is shown in Table 3. In order to determine the appropriate comparisons of the test statistics (F-test), the expected mean squares were derived based on the general algorithm [61]. The type of the effects, sum of squares, degree of freedoms, mean squares, the applied comparisons and p values are given in Table 3. The expected mean squares are summarized in Table S 3 (Appendix 1).

Based on the p values listed in Table 3, the effect of flow rate of the drying air, the mass flow rate and the L/S were significant factors ($p < 0.05$). Furthermore, the interaction between the flow rate of the drying air and the mass flow rate, the flow rate of the drying air and L/S, and the mass flow rate and the L/S were statistically significant. In this analysis, the higher-order interactions were neglected due to their presumably negligible effects on the response variable.

In order to facilitate the interpretation of the results of the DoE study, the response surfaces of the experiments are presented in Fig. 8a–d. As it can be observed, the increase of the flow rate of the drying air and the L/S resulted in higher levels of moisture content in the product in all cases. Similar surfaces were obtained on the different mass flow rate levels, only the scale of attainable moisture content differed. Examining the response surfaces from the different drying air temperature levels reveals that in this temperature range the attainable moisture content level was less dependent on this factor than on the others. The interaction of L/S and the flow rate of drying air was found to be significant during the statistical analysis of the results (Table 2), which is also visible in Fig. 8a–d as the surface is slightly curved.

As the ANOVA table shows (Table 3), the temperature of the drying air appeared to not have a significant effect on the measured moisture content at 0.05 significance level. Although, it should be noted that the p value of the effect of the temperature was very close to 0.05, thus this situation has not been fully clarified, yet. The sensitivity of the F-test concerning the temperature can be increased by greater sample size. To have a more detailed picture about this effect further experiments are planned in the future.

Since the temperature is known to play a fundamental role in the drying process [48], the first experimental design was extended with additional levels of drying air temperature as detailed in Section 2.7 by

Table 3
Results from ANOVA (split-plot design) for moisture content (%).

Effect[a]	Type of the effect[b]	Sum of square	Degree of freedom	Mean square	F_0	p
T	F	1.9769	1	1.9769	$\frac{s_T^2}{s_{B(T)}^2} = 10.98$	0.0803
B(T)[c]	R	0.3602	2	0.1801	–	–
D	F	7.5669	1	7.5669	$\frac{s_D^2}{s_{B(T)*D}^2} = 29.61$	**0.0321**
T*D	F	0.1057	1	0.1057	$\frac{s_{TD}^2}{s_{B(T)*D}^2} = 0.4137$	0.5860
B(T)*D	R	0.5111	2	0.2556	–	–
M	F	8.4165	1	8.4165	$\frac{s_M^2}{s_{B(T)*M}^2} = 737.4$	**0.0014**
T*M	F	0.0388	1	0.0388	$\frac{s_{TM}^2}{s_{B(T)*M}^2} = 3.399$	0.2066
B(T)*M	R	0.0228	2	0.0114	–	–
D*M	F	1.2812	1	1.2812	$\frac{s_{DM}^2}{s_{B(T)*D*M}^2} = 30.71$	**0.0116**
B(T)*D*M	R	0.1251	3	0.0417	–	–
L	F	22.3851	1	22.3851	$\frac{s_L^2}{s_{B(T)*L}^2} = 89.47$	**0.0110**
T*L	F	0.0082	1	0.0082	$\frac{s_{TL}^2}{s_{B(T)*L}^2} = 0.0328$	0.8726
B(T)*L	R	0.5004	2	0.2502	–	–
D*L	F	1.6000	1	1.6000	$\frac{s_{DL}^2}{s_{B(T)*D*L}^2} = 55.18$	**0.0051**
B(T)*D*L	R	0.0870	3	0.0029	–	–
M*L	F	2.5464	1	2.5464	$\frac{s_{ML}^2}{s_{B(T)*M*L}^2} = 42.39$	**0.0172**
B(T)*M*L	R	0.3319	3	0.1106	–	–
Error	–	0.9808	4	0.2452	–	–

[a] The abbreviations of the effects: T: temperature, B: block, D: flow rate of drying air, M: mass flow rate, L: L/S.
[b] The two types of effects: R: random or F: fixed.
[c] The B(T) notation means that the temperature is nested in the block factor.
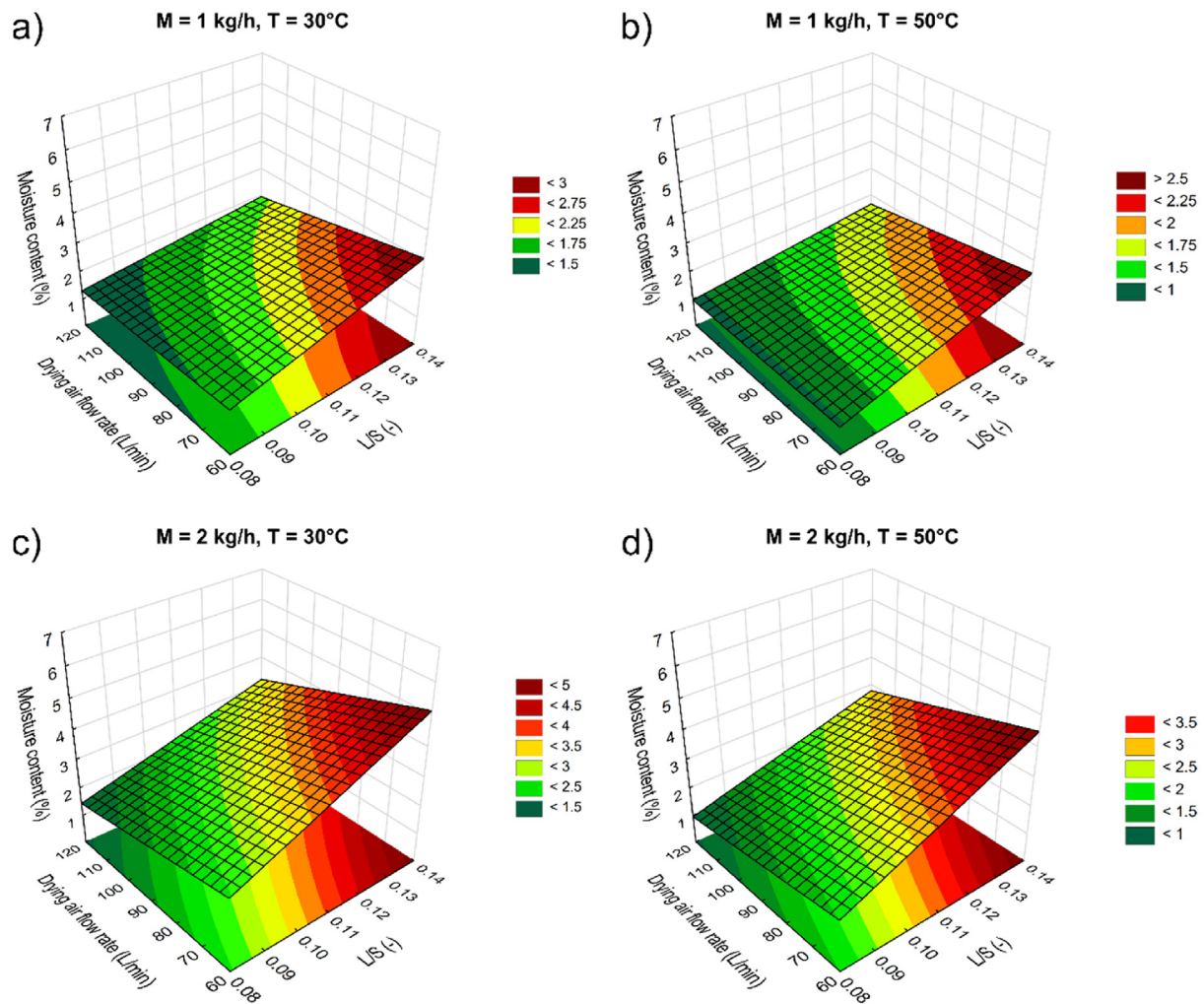
Fig. 8. Response surfaces of the split-plot experimental study. The settings of the other two factors are as follows: 1 kg/h mass flow rate – 30 °C temperature (a), 1 kg/h mass flow rate – 50 °C temperature (b), 2 kg/h mass flow rate – 30 °C temperature (c) and 2 kg/h mass flow rate – 50 °C temperature (d).

creating two new smaller 2^3 experimental designs at 70 °C and 90 °C. We did not include the results of these new blocks into the statistical analysis and DoE evaluation, since they were executed a longer period of time after the first DoE setup, leaving a possibility for additional variation. The results of the additional experiments are shown in Fig. 9.

Fig. 9 depicts that the measured moisture content is decreasing with the increasing temperature, dropping below 1% when *ca.* at 70 °C is reached. However, high moisture content was measured when the combination of the other three factors reduced the drying efficiency (high L/S and mass flow rate at both levels of drying air flow rate). This showed that the temperature alone could not decrease the residual moisture content level effectively even at this temperature level, however, it was possible to reach lower moisture contents than what was obtained at 50 °C. At 90 °C, the amount of remaining water was reduced below 1% in all cases; hence no effect could be observed for the other three factors. This result shows the importance of further evaluation of drying temperature on these higher levels.

3.3. Drying model

The unknown kinetic parameters of the mathematical model were determined based on the result of the DoE study. The obtained parameters and objective function values calculated for the calibration and validation datasets are listed in Table 4. As expected, the validation provides higher error than the calibration, however, there is no major

difference, indicating that there is no substantial overfitting. This is also underlined by the relatively narrow confidence intervals of the estimated parameters. For further details about the parameter estimation procedure, the reader is directed to Appendix 2.3.

The parity plot presenting the calibration and validation data is depicted in Fig. 10a. In addition to the nominal values, the simulated and measured SDs are plotted. There is a clear correlation between the measurements and the simulations, and the diagonal predominantly falls within the SD. Thus, the model is able to predict the product moisture content reasonably, and the SDs resulting from the parametric uncertainty are in the range of measurement SDs.

The validated model can provide detailed insight into the process. For example, Fig. 10b depicts the steady state temperature and moisture content profile along the dryer in a representative simulation. The drying air temperature is generally between 50 and 60 °C or 10–20 °C below its inlet temperature. The mean solid temperature remains well under the air temperature, due to the cooling effect of the evaporation. As expected, the moisture content decreases monotonically. The effects of the low temperature air stream in the last segment is clearly observable on both temperature curves that exhibit a sudden decrease, and on the slowing moisture content decrease, too. T_s shows higher SD than the moisture content, being influenced both by the uncertainties of evaporation rate and heat transfer parameters. The lower SD of T_a is explained by the higher air mass flow rate, which reduces the impact of the parameter uncertainty-caused heat uptake. Such simulations could be
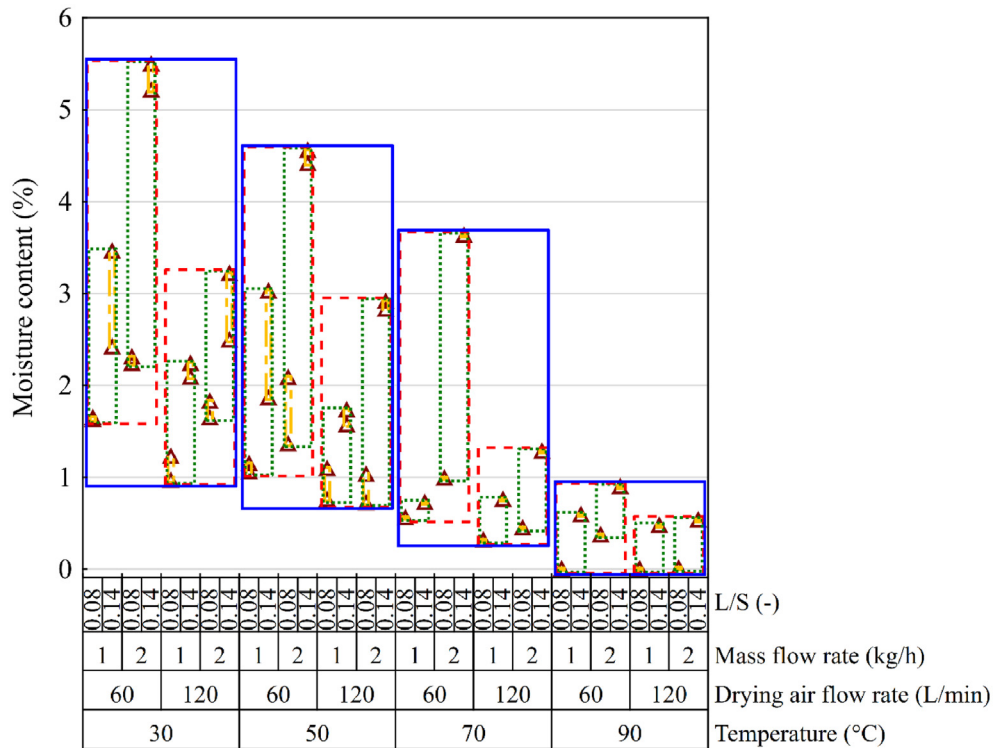
Fig. 9. Variability plot presenting the results of the split-plot experimental design supplemented with two more levels of drying temperature at 70 and 90 °C. Each setting is marked with a triangle, and the colored rectangles represent the higher and lower levels of the examined parameters (L/S: yellow rectangle with dash-dotted line; mass flow rate: green rectangle, dotted line; drying air flow rate: red rectangle, dashed line; temperature: blue rectangle, solid line). (For interpretation of the references to color in this figure legend, the reader is referred to the web version of this article.)

Table 4
Parameter estimation results: nominal parameters, 95% confidence interval bounds and objective function values.

Parameter	Name	Value
U	Heat transfer coefficient, W/(m²K)	0.106 (0.019, 1.93)
$\log(k)$	Evaporation rate constant, $\log(g/(s\,L))$	1.73 (0.73, 2.74)
$\log(E_A)$	Activation energy of evaporation, $\log(J/mol)$	8.52 (8.04, 9.00)
$\varphi_c(\boldsymbol{\theta})$	Objective function value, calibration dataset, %²	0.275
$\varphi_v(\boldsymbol{\theta})$	Objective function value, validation dataset, %²	0.735

performed in real-time, based on PAT sensor data, in which case numerous un-measured states become available from the simulation for process control and product property prediction.

There are several ways to improve the presented model, both in terms of estimated parameter accuracy and model structure. Some of the basic assumptions could be replaced with direct measurements *e.g.* the air pressure at the flow rate measurement; the relative humidity and temperature of the drying air leaving the dryer. Coupled with the temperature measurement of the solid material along the belt, this
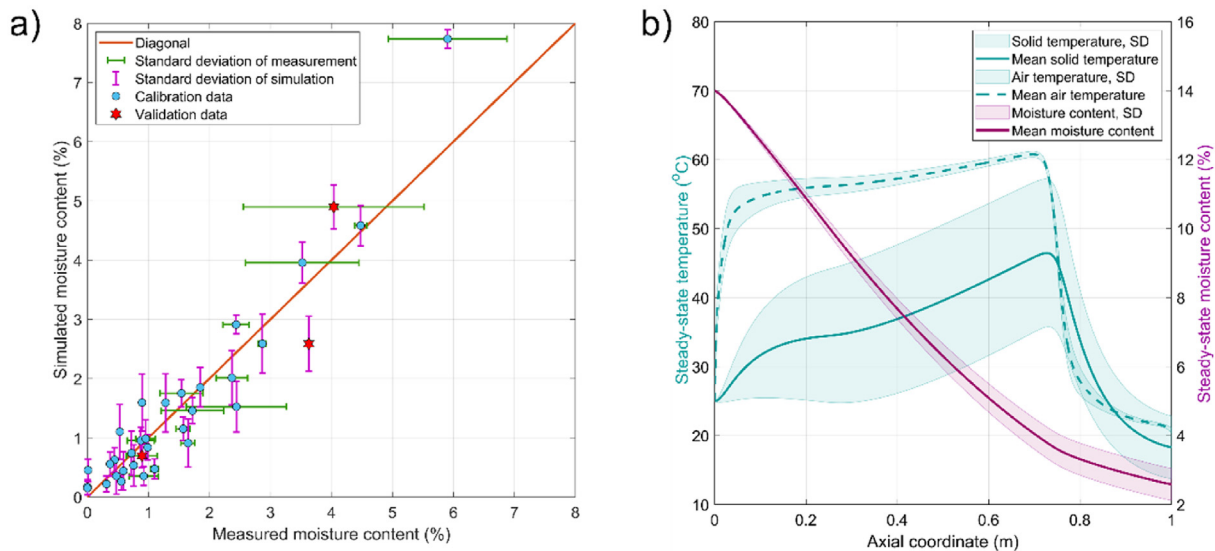

Fig. 10. a) Parity plot of steady state moisture content for the calibration and validation experiments. b) Simulated steady state temperature and moisture content profiles along the drying belt, together with the SDs resulting from the kinetic parameter uncertainties in a representative experiment with conditions: drying air temperature: 70 °C (25 °C in the last 0.25 m); drying air flow rate: 60 L/min; solid flow rate: 2 kg/h; L/S = 0.14.
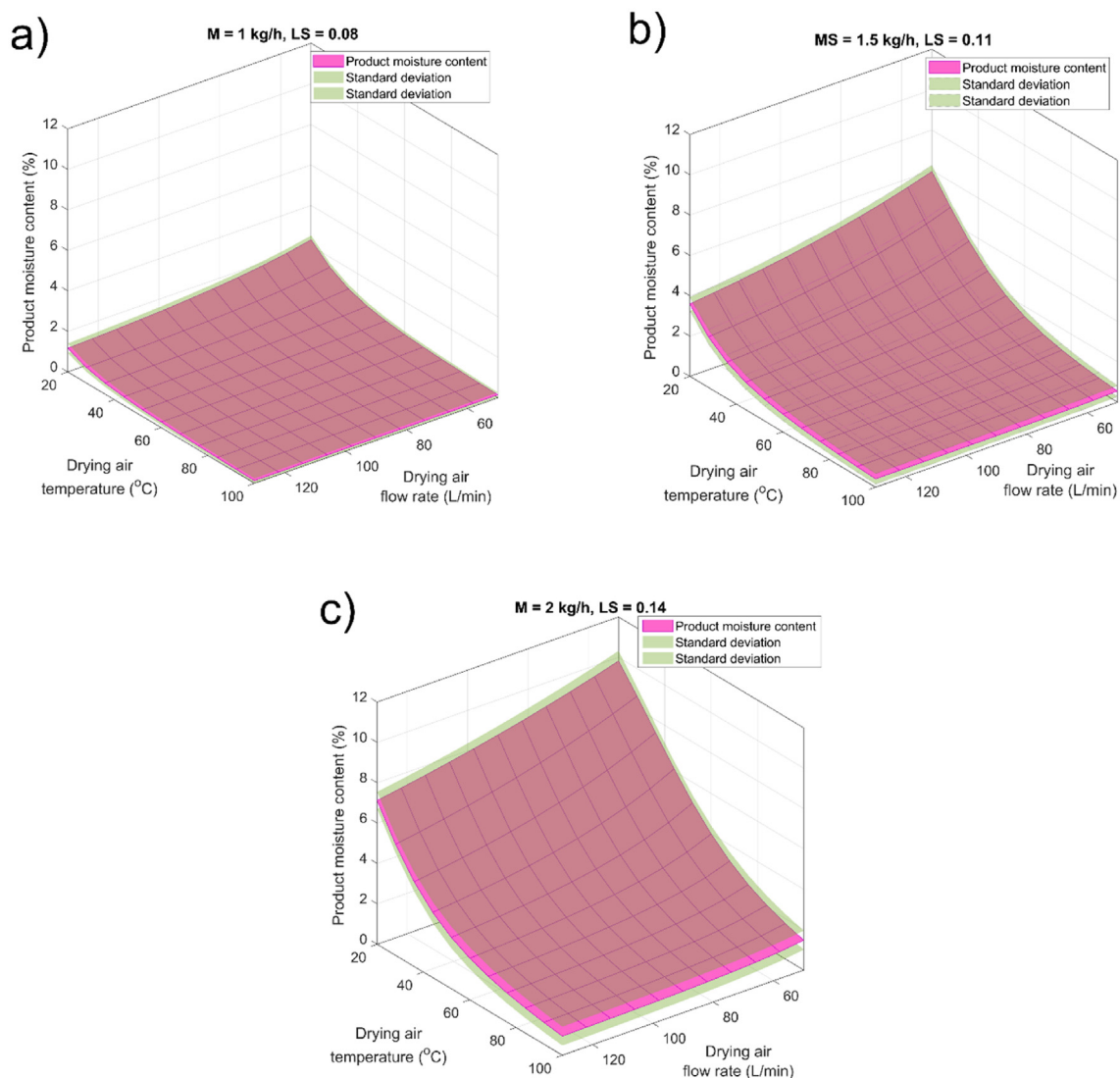
Fig. 11. Simulation study for the determination of achievable product moisture content in the typical dryer operating range at a) low, b) medium and c) high moisture contents.

would allow not only to de-couple the heat transfer coefficient and the drying rate (reducing the SD of T_s) but also to estimate more model parameters, such as X_c. The specific surface area of the powder belonging to various twin-screw granulator operating conditions could be determined, enabling more accurate gas-solid heat and mass transfer calculation. From a model structure perspective, one may describe the evaporation rate as a two-step process, accounting for the kinetics of water diffusion from the pores to the surface of particles. From a mathematical perspective, dynamic information could easily be obtained, which is alluring but it would also require dynamic model calibration.

Once a model with quantified prediction capability and uncertainty becomes available, it can be used for various purposes. In this work, the achievable product moisture content domains are investigated for three characteristic L/S ratios and solid mass flow rates. The operating conditions were varied in the region of experimental conditions, with slight extrapolation (50–130 L/min in the simulation study *vs.* 60–120 L/min in the experiments, and 20–100 °C in the simulation study *vs.* 30–90 °C in the experiments). The results are depicted in Fig. 11a–c. When both the initial moisture and mass flow rate are high, significantly higher product moistures are realized than in the mid-, and low-level cases (2–10%, ~1–6% and ~ 0–3%, respectively). Unsurprisingly, the lowest product moisture content was predicted at the highest drying air temperature and flow rate in all cases, and *vice-versa*. It is noteworthy

that at sufficiently high drying air flow rates, regardless its temperature, sufficiently low moisture contents can be achieved (<2%) (Fig. 11c). This observation aligns with the outcomes of the experimental design and has great significance in the drying of heat-sensitive APIs.

4. Conclusions

In this work a deep and thorough process understanding approach was presented for integrated continuous pharmaceutical technologies. The process performance of a TSWG-FBD-milling line was evaluated rapidly by means of mechanistic modeling and design of experiments using real-time PAT monitoring. A PLS model was built using NIR spectroscopy for the real-time monitoring of the moisture content of the dried and milled product. The NIR calibration model was found to be accurate and reliable, with a 0.168% prediction error RMSEP. A full factorial split-plot experimental design was executed within just a few hours to assess the effect of process parameters on the residual water content of the granules. It was found that the mass flow rate of the starting pre-blend, the L/S and the flow rate of the drying air are statistically significant variables. The temperature of the drying air was also important; however, the *p* value was close but did not reach the 0.05 significance criteria. This was the motivation to extend the studied temperature range. These experiments revealed that at a high drying air

temperature, the moisture content falls below 1% regardless of any other parameters, but sufficiently high drying air flow rates could result in low moisture contents even at low air temperatures. This is an important observation for the drying of thermolabile APIs. A mechanistic process model was developed and calibrated based on the experimental data recorded as a part of the DoE. The simulation results reinforced the experimental observations.

Using the developed model, the number of experiments required for process understanding can be decreased in future works, but it also paves the way for the process optimizations and applications of digital twins. In conclusion, it was presented in this study that comprehensive and thorough process understanding can be achieved within a short time by PAT-supported DoE studies supported by digital twin-based simulations, which could bring QbD-based process development to a new level.

Declaration of Competing Interest

The authors declare no conflict of interest.

Acknowledgements

Appendix A. Supplementary data

Supplementary data to this article can be found online at https://doi.org/10.1016/j.powtec.2021.04.059.

References

[1] C.L. Burcham, A.J. Florence, M.D. Johnson, Continuous manufacturing in pharmaceutical process development and manufacturing, Annu. Rev. Chem. Biomol. Eng. 9 (2018) 253–281, https://doi.org/10.1146/annurev-chembioeng-060817-084355.

[2] S.L. Lee, T.F. O'Connor, X. Yang, C.N. Cruz, S. Chatterjee, R.D. Madurawe, C.M.V. Moore, L.X. Yu, J. Woodcock, Modernizing pharmaceutical manufacturing: from batch to continuous production, J. Pharm. Innov. 10 (2015) 191–199, https://doi.org/10.1007/s12247-015-9215-8.

[3] V. Vanhoorne, C. Vervaet, Recent progress in continuous manufacturing of oral solid dosage forms, Int. J. Pharm. 579 (2020) 119194, https://doi.org/10.1016/j.ijpharm.2020.119194.

[4] M. Fonteyne, D. Gildemyn, E. Peeters, S.T.F.C. Mortier, J. Vercruysse, K.V. Gernaey, C. Vervaet, J.P. Remon, I. Nopens, T. De Beer, Moisture and drug solid-state monitoring during a continuous drying process using empirical and mass balance models, Eur. J. Pharm. Biopharm. 87 (2014) 616–628, https://doi.org/10.1016/j.ejpb.2014.02.015.

[5] P. Thapa, J. Tripathi, S.H. Jeong, Recent trends and future perspective of pharmaceutical wet granulation for better process understanding and product development, Powder Technol. 344 (2019) 864–882, https://doi.org/10.1016/j.powtec.2018.12.080.

[6] C. Vervaet, J.P. Remon, Continuous granulation in the pharmaceutical industry, Chem. Eng. Sci. 60 (2005) 3949–3957, https://doi.org/10.1016/j.ces.2005.02.028.

[7] R.M. Dhenge, J.J. Cartwright, M.J. Hounslow, A.D. Salman, Twin screw wet granulation: effects of properties of granulation liquid, Powder Technol. 229 (2012) 126–136, https://doi.org/10.1016/j.powtec.2012.06.019.

[8] J. Vercruysse, D. Córdoba Díaz, E. Peeters, M. Fonteyne, U. Delaet, I. Van Assche, T. De Beer, J.P. Remon, C. Vervaet, Continuous twin screw granulation: influence of process variables on granule and tablet quality, Eur. J. Pharm. Biopharm. 82 (2012) 205–211, https://doi.org/10.1016/j.ejpb.2012.05.010.

[9] S. Bandari, D. Nyavanandi, V.R. Kallakunta, K.Y. Janga, S. Sarabu, A. Butreddy, M.A. Repka, Continuous twin screw granulation – an advanced alternative granulation technology for use in the pharmaceutical industry, Int. J. Pharm. 580 (2020) 119215, https://doi.org/10.1016/j.ijpharm.2020.119215.

[10] A. Ito, P. Kleinebudde, Influence of granulation temperature on particle size distribution of granules in twin-screw granulation (TSG), Pharm. Dev. Technol. 24 (2019) 874–882, https://doi.org/10.1080/10837450.2019.1615089.

[11] R.M. Dhenge, R.S. Fyles, J.J. Cartwright, D.G. Doughty, M.J. Hounslow, A.D. Salman, Twin screw wet granulation: granule properties, Chem. Eng. J. 164 (2010) 322–329, https://doi.org/10.1016/j.cej.2010.05.023.

[12] L.J. Gorringe, G.S. Kee, M.F. Saleh, N.H. Fa, R.G. Elkes, Use of the channel fill level in defining a design space for twin screw wet granulation, Int. J. Pharm. 519 (2017) 165–177, https://doi.org/10.1016/j.ijpharm.2017.01.029.

[13] J. Vercruysse, A. Burggraeve, M. Fonteyne, P. Cappuyns, U. Delaet, I. Van Assche, T. De Beer, J.P. Remon, C. Vervaet, Impact of screw configuration on the particle size distribution of granules produced by twin screw granulation, Int. J. Pharm. 479 (2015) 171–180, https://doi.org/10.1016/j.ijpharm.2014.12.071.

[14] R. Meier, K.-P. Moll, M. Krumme, P. Kleinebudde, Impact of fill-level in twin-screw granulation on critical quality attributes of granules and tablets, Eur. J. Pharm. Biopharm. 115 (2017) 102–112, https://doi.org/10.1016/j.ejpb.2017.02.010.

[15] N. Nicolaï, F. De Leersnyder, D. Copot, M. Stock, C.M. Ionescu, K.V. Gernaey, I. Nopens, T. De Beer, Liquid-to-solid ratio control as an advanced process control solution for continuous twin-screw wet granulation, AICHE J. 64 (2018) 2500–2514, https://doi.org/10.1002/aic.16161.

[16] D. Djuric, P. Kleinebudde, Impact of screw elements on continuous granulation with a twin-screw extruder, J. Pharm. Sci. 97 (2008) 4934–4942, https://doi.org/10.1002/jps.21339.

[17] S. Lute, R. Dhenge, A. Salman, Twin screw granulation: an investigation of the effect of barrel fill level, Pharmaceutics 10 (2018) 67, https://doi.org/10.3390/pharmaceutics10020067.

[18] H. Li, M.R. Thompson, K.P. O'Donnell, Understanding wet granulation in the kneading block of twin screw extruders, Chem. Eng. Sci. 113 (2014) 11–21, https://doi.org/10.1016/j.ces.2014.03.007.

[19] C. Portier, K. Pandelaere, U. Delaet, T. Vigh, A. Kumar, G. Di Pretoro, T. De Beer, C. Vervaet, V. Vanhoorne, Continuous twin screw granulation: influence of process and formulation variables on granule quality attributes of model formulations, Int. J. Pharm. 576 (2020) 118981, https://doi.org/10.1016/j.ijpharm.2019.118981.

[20] C. Portier, K. Pandelaere, U. Delaet, T. Vigh, G. Di Pretoro, T. De Beer, C. Vervaet, V. Vanhoorne, Continuous twin screw granulation: a complex interplay between formulation properties, process settings and screw design, Int. J. Pharm. 576 (2020) 119004, https://doi.org/10.1016/j.ijpharm.2019.119004.

[21] C. Portier, T. Vigh, G. Di Pretoro, T. De Beer, C. Vervaet, V. Vanhoorne, Continuous twin screw granulation: impact of binder addition method and surfactants on granulation of a high-dosed, poorly soluble API, Int. J. Pharm. 577 (2020) 119068, https://doi.org/10.1016/j.ijpharm.2020.119068.

[22] A.S. El Hagrasy, J.R. Hennenkamp, M.D. Burke, J.J. Cartwright, J.D. Litster, Twin screw wet granulation: influence of formulation parameters on granule properties and growth behavior, Powder Technol. 238 (2013) 108–115, https://doi.org/10.1016/j.powtec.2012.04.035.

[23] G. Dahlgren, P. Tajarobi, E. Simone, B. Ricart, J. Melnick, V. Puri, C. Stanton, G. Bajwa, Continuous twin screw wet granulation and drying—control strategy for drug product manufacturing, J. Pharm. Sci. 108 (2019) 3502–3514, https://doi.org/10.1016/j.xphs.2019.06.023.

[24] V. Pauli, F. Elbaz, P. Kleinebudde, M. Krumme, Orthogonal redundant monitoring of a new continuous fluid-bed dryer for pharmaceutical processing by means of mass and energy balance calculations and spectroscopic techniques, J. Pharm. Sci. 108 (2019) 2041–2055, https://doi.org/10.1016/j.xphs.2018.12.028.

[25] J. Vercruysse, U. Delaet, I. Van Assche, P. Cappuyns, F. Arata, G. Caporicci, T. De Beer, J.P. Remon, C. Vervaet, Stability and repeatability of a continuous twin screw granulation and drying system, Eur. J. Pharm. Biopharm. 85 (2013) 1031–1038, https://doi.org/10.1016/j.ejpb.2013.05.002.

[26] J. Vercruysse, E. Peeters, M. Fonteyne, P. Cappuyns, U. Delaet, I. Van Assche, T. De Beer, J.P. Remon, C. Vervaet, Use of a continuous twin screw granulation and drying system during formulation development and process optimization, Eur. J. Pharm. Biopharm. 89 (2015) 239–247, https://doi.org/10.1016/j.ejpb.2014.12.017.

[27] J. Palmer, C.J. O'Malley, M.J. Wade, E.B. Martin, T. Page, G.A. Montague, Opportunities for process control and quality assurance using online NIR analysis to a continuous wet granulation tableting line, J. Pharm. Innov. 15 (2020) 26–40, https://doi.org/10.1007/s12247-018-9364-7.

[28] J. Menth, M. Maus, K.G. Wagner, Continuous twin screw granulation and fluid bed drying: a mechanistic scaling approach focusing optimal tablet properties, Int. J. Pharm. 586 (2020) 119509, https://doi.org/10.1016/j.ijpharm.2020.119509.

[29] V. Pauli, F. Elbaz, P. Kleinebudde, M. Krumme, Methodology for a variable rate control strategy development in continuous manufacturing applied to twin-screw wet-granulation and continuous fluid-bed drying, J. Pharm. Innov. 13 (2018) 247–260, https://doi.org/10.1007/s12247-018-9320-6.

[30] J. Peters, A. Teske, W. Taute, C. Döscher, M. Höft, R. Knöchel, J. Breitkreutz, Real-time process monitoring in a semi-continuous fluid-bed dryer – microwave resonance technology versus near-infrared spectroscopy, Int. J. Pharm. 537 (2018) 193–201, https://doi.org/10.1016/j.ijpharm.2017.12.040.

[31] S. Devahastin, in: Christopher G.J. Baker (Ed.), Review of: "Industrial Drying of Foods", Blackie Academic & Professional, London, UK, 1997, https://doi.org/10.1080/07373939808917446 , 309 pages, Dry. Technol. 16 (1998) 917–918.

[32] A.S. Mujumdar, K. Erdesz, Applications of vibration techniques for drying and agglomeration in food processing, Dry. Technol. 6 (1988) 255–274, https://doi.org/10.1080/07373938808916375.

[33] R. Meier, Continuous Wet Granulation and Fluid-Bed Drying – An Experimental Investigation of a New Revolutionary System, https://www.continuous-production.com/images/QbCon_1/QbCon_1_continuous_drying.pdf 2018.

[34] Y. Roggo, V. Pauli, M. Jelsch, L. Pellegatti, F. Elbaz, S. Ensslin, P. Kleinebudde, M. Krumme, Continuous manufacturing process monitoring of pharmaceutical solid dosage form: a case study, J. Pharm. Biomed. Anal. 179 (2020) 112971, https://doi.org/10.1016/j.jpba.2019.112971.

[35] S. Laske, A. Paudel, O. Scheibelhofer, S. Sacher, T. Hoermann, J. Khinast, A. Kelly, J. Rantannen, O. Korhonen, F. Stauffer, F. De Leersnyder, T. De Beer, J. Mantanus, P.-F. Chavez, B. Thoorens, P. Ghiotti, M. Schubert, P. Tajarobi, G. Haeffler, S. Lakio, M. Fransson, A. Sparen, S. Abrahmsen-Alami, S. Folestad, A. Funke, I. Backx, B. Kavsek, F. Kjell, M. Michaelis, T. Page, J. Palmer, A. Schaepman, S. Sekulic, S. Hammond, B. Braun, B. Colegrove, A review of PAT strategies in secondary solid oral dosage manufacturing of small molecules, J. Pharm. Sci. 106 (2017) 667–712, https://doi.org/10.1016/j.xphs.2016.11.011.

[36] M. Fonteyne, J. Vercruysse, F. De Leersnyder, B. Van Snick, C. Vervaet, J.P. Remon, T. De Beer, Process analytical technology for continuous manufacturing of solid-dosage forms, TrAC Trends Anal. Chem. 67 (2015) 159–166, https://doi.org/10.1016/j.trac.2015.01.011.

[37] L. Madarász, Z.K. Nagy, I. Hoffer, B. Szabó, I. Csontos, H. Pataki, B. Démuth, B. Szabó, K. Csorba, G. Marosi, Real-time feedback control of twin-screw wet granulation based on image analysis, Int. J. Pharm. 547 (2018) 360–367, https://doi.org/10.1016/j.ijpharm.2018.06.003.

[38] J. Harting, P. Kleinebudde, Development of an in-line Raman spectroscopic method for continuous API quantification during twin-screw wet granulation, Eur. J. Pharm. Biopharm. 125 (2018) 169–181, https://doi.org/10.1016/j.ejpb.2018.01.015.

[39] W. Meng, A.D. Román-Ospino, S.S. Panikar, C. O'Callaghan, S.J. Gilliam, R. Ramachandran, F.J. Muzzio, Advanced process design and understanding of continuous twin-screw granulation via implementation of in-line process analytical technologies, Adv. Powder Technol. 30 (2019) 879–894, https://doi.org/10.1016/j.apt.2019.01.017.

[40] M. Fonteyne, J. Vercruysse, D.C. Díaz, D. Gildemyn, C. Vervaet, J.P. Remon, T. De Beer, Real-time assessment of critical quality attributes of a continuous granulation process, Pharm. Dev. Technol. 18 (2013) 85–97, https://doi.org/10.3109/10837450.2011.627869.

[41] M. Fonteyne, J. Arruabarrena, J. de Beer, M. Hellings, T. Van Den Kerkhof, A. Burggraeve, C. Vervaet, J.P. Remon, T. De Beer, NIR spectroscopic method for the in-line moisture assessment during drying in a six-segmented fluid bed dryer of a continuous tablet production line: validation of quantifying abilities and uncertainty assessment, J. Pharm. Biomed. Anal. 100 (2014) 21–27, https://doi.org/10.1016/j.jpba.2014.07.012.

[42] L. Chablani, M.K. Taylor, A. Mehrotra, P. Rameas, W.C. Stagner, Inline real-time near-infrared granule moisture measurements of a continuous granulation–drying–milling process, AAPS PharmSciTech 12 (2011) 1050–1055, https://doi.org/10.1208/s12249-011-9669-z.

[43] M. Fonteyne, S. Soares, J. Vercruysse, E. Peeters, A. Burggraeve, C. Vervaet, J.P. Remon, N. Sandler, T. De Beer, Prediction of quality attributes of continuously produced granules using complementary pat tools, Eur. J. Pharm. Biopharm. 82 (2012) 429–436, https://doi.org/10.1016/j.ejpb.2012.07.017.

[44] D.J. Lamberto, J. Neuhaus, Robust process scale-up leveraging design of experiments to map active pharmaceutical ingredient humid drying parameter space, Org. Process Res. Dev. 0 (2021), https://doi.org/10.1021/acs.oprd.0c00475.

[45] D. Leitold, Á. Vathy-Fogarassy, J. Abonyi, Network-Based Analysis of Dynamical Systems, Springer International Publishing, Cham, 2020, https://doi.org/10.1007/978-3-030-36472-4.

[46] G. Fülöp, A. Domokos, D. Galata, E. Szabó, M. Gyürkés, B. Szabó, A. Farkas, L. Madarász, B. Démuth, T. Lendér, T. Nagy, D. Kovács-Kiss, F. Van der Gucht, G. Marosi, Z.K. Nagy, Integrated twin-screw wet granulation, continuous vibrational fluid drying and milling: a fully continuous powder to granule line, Int. J. Pharm. 594 (2021) 120126, https://doi.org/10.1016/j.ijpharm.2020.120126.

[47] J. Rehrl, S. Sacher, M. Horn, J. Khinast, End-point prediction of granule moisture in a ConsiGmaTM-25 segmented fluid bed dryer, Pharmaceutics 12 (2020) 452, https://doi.org/10.3390/pharmaceutics12050452.

[48] D.R. Ochsenbein, M. Billups, B. Hong, E. Schäfer, A.J. Marchut, O.K. Lyngberg, Industrial application of heat- and mass balance model for fluid-bed granulation for technology transfer and design space exploration, Int. J. Pharm. X 1 (2019) 100028, https://doi.org/10.1016/j.ijpx.2019.100028.

[49] R.M.C. Portela, C. Varsakelis, A. Richelle, N. Giannelos, J. Pence, S. Dessoy, M. von Stosch, When Is an in Silico Representation a Digital Twin? A Biopharmaceutical Industry Approach to the Digital Twin Concept, 2020, https://doi.org/10.1007/10_2020_138.

[50] A. Elkhashap, R. Meier, D. Abel, A grey box distributed parameter model for a continuous vibrated fluidized bed dryer in pharmaceutical manufacturing, 2020 Eur. Control Conf., IEEE 2020, pp. 1415–1421, https://doi.org/10.23919/ECC51009.2020.9143770.

[51] S.T.F.C. Mortier, K.V. Gernaey, T. De Beer, I. Nopens, Analysing drying unit performance in a continuous pharmaceutical manufacturing line by means of mass – energy balances, Eur. J. Pharm. Biopharm. 86 (2014) 532–543, https://doi.org/10.1016/j.ejpb.2013.12.014.

[52] P. Rahimi Borujerdi, B. Shotorban, S. Mahalingam, D.R. Weise, Modeling of water evaporation from a shrinking moist biomass slab subject to heating: Arrhenius approach versus equilibrium approach, Int. J. Heat Mass Transf. 145 (2019) 118672, https://doi.org/10.1016/j.ijheatmasstransfer.2019.118672.

[53] S. Ottoboni, S.J. Coleman, C. Steven, M. Siddique, M. Fraissinet, M. Joannes, A. Laux, A. Barton, P. Firth, C.J. Price, P.A. Mulheran, Understanding API static drying with hot gas flow: design and test of a drying rig prototype and drying modeling development, Org. Process. Res. Dev. 24 (2020) 2505–2520, https://doi.org/10.1021/acs.oprd.0c00035.

[54] D.J. Ende, M.T. Ende (Eds.), Chemical Engineering in the Pharmaceutical Industry, Wiley, 2019, https://doi.org/10.1002/9781119600800.

[55] B. Szilagyi, A. Eren, J.L. Quon, C.D. Papageorgiou, Z.K. Nagy, Application of model-free and model-based quality-by-control (QbC) for the efficient design of pharmaceutical crystallization processes, Cryst. Growth Des. 20 (2020) 3979–3996, https://doi.org/10.1021/acs.cgd.0c00295.

[56] F. Gagnon, J. Bouchard, A. Desbiens, É. Poulin, Development and validation of a batch fluidized bed dryer model for pharmaceutical particles, Dry. Technol. 39 (2021) 620–643, https://doi.org/10.1080/07373937.2019.1701005.

[57] Y.C. Liu, D. Acevedo, X. Yang, S. Naimi, W.-L. Wu, N. Pavurala, Z.K. Nagy, T.F. O'Connor, Population balance model development verification and validation of cooling crystallization of carbamazepine, Cryst. Growth Des. 20 (2020) 5235–5250, https://doi.org/10.1021/acs.cgd.0c00434.

[58] N. Hansen, S.D. Müller, P. Koumoutsakos, Reducing the time complexity of the derandomized evolution strategy with covariance matrix adaptation (CMA-ES), Evol. Comput. 11 (2003) 1–18, https://doi.org/10.1162/106365603321828970.

[59] Z.K. Nagy, R.D. Braatz, Distributional uncertainty analysis using power series and polynomial chaos expansions, J. Process Control 17 (2007) 229–240, https://doi.org/10.1016/j.jprocont.2006.10.008.

[60] T. Afrin, S.N. Karobi, M.M. Rahman, M.Y.A. Mollah, M.A.B.H. Susan, Water structure modification by sugars and its consequence on micellization behavior of cetyltrimethylammonium bromide in aqueous solution, J. Solut. Chem. 42 (2013) 1488–1499, https://doi.org/10.1007/s10953-013-0050-6.

[61] T. Lorenzen, Design of Experiments, CRC Press, 1993, https://doi.org/10.1201/9781482277524.

Nomenclature

R_v:	drying rate, g/s
U:	overall heat transfer coefficient between the solid and gas phases, J/(m²s °C)
A:	total heat transfer area, m²
T_a:	air temperature, °C
T_s:	solid temperature, °C
$T_{s,K}$:	solid temperature, K
R:	gas constant, J/(mol K)
k:	drying rate constant, g/s
E_A:	drying rate activation energy, J/mol
k_0:	pre-exponential factor, g/s
H_r:	relative humidity of the air, —
X:	moisture content, %
X_C:	critical moisture content, %
P_A:	water pressure, atm
P_A^*:	saturation water pressure, atm
Q:	gas-solid heat transfer rate, J/s
N:	number of experiments used in the model parameter estimation, —
F_a:	air flowrate, g/s
n:	probability density function, —
L:	axial coordinate, m
P_g:	0.9th percentile of q, —
T_M:	upper limit of desired solid temperature, °C
X_M:	upper limit of desired product moisture range, %
T:	temperature, °C
B:	block, —
D:	flow rate of drying air, L/min
M:	mass flow rate, kg/h
L:	L/S, —
Φ:	fixed effect of the factors
σ^2:	variance of the random effect of the factors

Greek letters

θ:	decision variable vector,
φ:	goal function of optimization,
ω:	vector of operating conditions,

Subscript

e:	experimental
s:	solid - simulation
a:	air
t:	total drier length